24th COBEM - 2017

24th ABCM International Congress of Mechanical Engineering
December 3-8, 2017, Curitiba, PR, Brazil

COBEM-2017-1022
AN ALE-FEM METHOD FOR AXISYMMETRIC TWO-PHASE FLOWS

Erik Gros
John. R. Thome
Laboratory of Heat and Mass Transfer - LTCM École Polytechnique Fédérale de Lausanne EPFL-STI-IGM-LTCM, Station 9, CH-1015, Lausanne, Switzerland
erik.gros@epfl.ch, john.thome@epfl.ch

Gustavo R. Anjos
State University of Rio de Janeiro - UERJ, R. Fonseca Teles 524, 20550-013, Rio de Janeiro, Brazil
gustavo.anjos@uerj.br

Abstract.
The present work aims at developing a computational framework to simulate macro and microscale two-phase flows in axisymmetric coordinates. An important application is the microchannels that will be used for the cooling of next generation micro-electronics and flows in biological systems. Several flow regimes can be found in those channels such as annular flow, slug flow with small and large bubbles and single bubble flows. All regimes are characterised by a thin interface seprating fluids. Therefore, an accurate method capable of capturing the wall/interface dynamics is strictly required. In this article an interface tracking Finite Element Method (FEM) is used to solve the equations governing the motion of two in-miscible incompressible fluids. This method describes the interface between the different fluids by a layer of zero thickness, which makes it highly accurated. At the scale of interest, surface tension plays an important role and is thus considered in the equations. An in-house code, previously implemented by Anjos (2012); Anjos et al. *(2014b,a), is further developed and presently extended first to better model microchannel flows. This paper will present tests and validations of the current axisymmetric code in comparison with large used benchmarks.*

Keywords: *interface, arbitrary Lagrangian-Eulerian, Finite Element Method, Rayleigh-Taylor instability, rising bubble*

1. INTRODUCTION

Two-phase flow occurs frequently in nature and in industrial applications. This is for instance the case in the refrigeration industry or lately in the cooling of computer chips and power electronics. Two-phase cooling systems are usually superior to single-phase cooling systems. This is given by the fact that for most materials the latent heat of va- porization is much higher than the thermal capacity of the liquid. The development of design tools for two-phase microchannels is becoming an important area of research. However, experiments are difficult to perform to investigate the dynamic nature of these flows because of the very small scales and numerical simulations offer an alternative way to study such flows usually at a much lower cost. Therefore, the development of numerical methods able to simulate these flows is an important research goal.

The Finite Element Method (FEM) opens new ways in both interface tracking as well as interface capturing. Space time methods Masud (1997); Tezduyar (1992) use finite elements to discretize both the spatial and time domain. They thereby allow for another kind of interface tracking where the deformation of the computational mesh is automatically included in the problem formulation. Meanwhile the eXtended Finite Element Method (XFEM) is ushering in a renaissance in Eulerian (fixed grid) two-phase flow. The XFEM is based on the idea of adding extra degrees of freedom to the fixed mesh problem, which are interpolated by discontinuous functions inside elements traversed by the interface. However, the XFEM approach suffers from ill conditioning of the associated discrete linear operator, which makes the solution of the linear system a more delicate task Sauerland (2013).

All interface tracking methods require remeshing to handle cases where the motion of the interface leads to strong mesh distortions. Remeshing can mean changing not only the connectivity of the mesh points but also inserting/removing mesh points. Therefore, after remeshing, an interpolation is required to project the solution onto the new mesh. This interpolation leads to additional numerical errors, which are usually of diffusive nature. Some authors propose changing only the connectivity, e.g. by swapping edges or performing operations locally to avoid global remeshing Quan (2007). However, these techniques lead to frequent insertion/deletion operations on vectors, which typically require doubly or single linked lists to perform better and may become less efficient than global remeshing. In Murea (2010) it is shown

for some simple academic problems that remeshing at every time step can be more accurate than using an ALE scheme without remeshing. This is due to the fact that remeshing allows the mesh resolution to be increased by adding more points to the mesh. This can be used dynamically to refine the mesh in regions where refinement is needed and coarsen the mesh elsewhere.

In this paper an interface tracking method, which accurately captures capillary effects and is able to handle cases with large interface deformations, is presented. The method presented here uses boundary-adapted grids, where the grid points at the interface are moved along with the flow velocity in Lagrangian fashion while the grid points on the boundaries of the domain remain fixed in Eulerian fashion. By a sophisticated motion of the grid points which are neither on the interface nor on the boundaries this method reaches a accurate description of the interface at any time, while avoiding the strong mesh distortion of purely Lagrangian methods. Adaptive mesh refinement and remeshing are used to keep a good quality mesh. An efficient way to compute the curvature and the surface tension term is used as described in Gros *et al.*. Results and validations in axisymmetric geometries are presented.

2. EQUATIONS IN AXISYMMETRIC FORMULATION

In the present work an interface tracking method will be used together with point insertion/deletion algorithms to maintain a suitable mesh quality. Different criteria are implemented to control the local mesh refinement. The principal criterion is based on a target edge size which is a field (just like the flow quantities), i.e. defined for every mesh point. This target edge size is computed by solving a Helmholtz equation to make sure that its variations are smooth, see Anjos *et al.* (2014a) for more details. Additionally, some geometrical refinement criteria are also used, for example point insertion close to the interface can be controlled by the interface curvature.

The classical description of two-phase flow is based on the governing equations of continuum mechanics of flowing media or hydrodynamics. These are the incompressible Navier-Stokes equations including surface tension in axisymmetric formulation:

$$\rho(x)\frac{D\mathbf{v}}{Dt} = -\nabla p + \frac{1}{N^{1/2}}\mu(x)\begin{bmatrix} 2\frac{1}{r}\frac{\partial}{\partial r}r\frac{\partial}{\partial r}v + \frac{\partial}{\partial x}\frac{\partial u}{\partial r} + \frac{\partial^2 v}{\partial^2 r} - \frac{2u}{r} \\ \frac{1}{r}\frac{\partial}{\partial r}r\frac{\partial}{\partial r}u + \frac{1}{r}\frac{\partial}{\partial r}r\frac{\partial}{\partial x}v + 2\frac{\partial^2 u}{\partial^2 x} \end{bmatrix} + \rho(x)\mathbf{g} + \frac{1}{Eo}\mathbf{f_{st}} \tag{1}$$

$$\frac{\partial u}{\partial x} + \frac{\partial v}{\partial r} + \frac{v}{r} = 0 \tag{2}$$

where $\rho(x)$ and $\mu(x)$ stand for the density and viscosity of the fluids in the numerical domain as a function of the position occupied by the fluid, $\mathbf{v}$ is the velocity field in axisymmetric coordinates with axial u and radial v components, t represents time, p pressure, $\mathbf{g}$ is gravity and $\mathbf{f_{st}}$ represents the surface tension force according to Brackbill and Kothe (1992) and modeled as:

$$\mathbf{f_{st}} = \kappa\nabla H \tag{3}$$

where κ stand for curvature and ∇H is the gradient of the Heaviside function H, which is equal to one in the inner phase and zero in the outer phase. The non-dimensional numbers Archimedes N and Eötvös Eo are both defined as:

$$N = \frac{\rho_0^2 g_0 D^3}{\mu_0^2} \qquad\qquad Eo = \frac{\rho_0 g_0 D^2}{\sigma_0}$$

note that the above non-dimensional groups are achieved by using the standard parameters when the velocity of the system is unknown, thus replacing the common non-dimensionalization $u^* = u/U_0$ by $\mathbf{u}^* = \mathbf{u}/\sqrt{g_0 D_0}$ and $\mathbf{x}^* = \mathbf{x}/L$ by $\mathbf{x}^* = \mathbf{x}/D$, where U_0, L and D are referential parameters of velocity, length and tube diameter respectively and $*$ stands for the non-dimensional quantities. Additionally, the non-dimensional Morton number and Capillary number are defined due to their importance to characterize the shape of a bubble or (drop) and the relative effect of the viscous and surface tension forces, respectively:

$$Mo = \frac{\mu_0^4 g_0}{\rho_0 \sigma_0^3} = Eo^3 N^2 \qquad\qquad Ca = \frac{\mu_0 U_0}{\sigma_0}$$

The material derivative $D\mathbf{v}/Dt$ is defined in the Arbitrary Eulerian-Lagrangian framework as follows:

$$\frac{D\mathbf{v}}{Dt} = \frac{\partial \mathbf{v}}{\partial t} + \mathbf{c}\cdot\nabla\mathbf{v} \tag{4}$$

where $\mathbf{c}$ represents the difference between the fluid flow $\mathbf{v}$ and the mesh velocity $\hat{\mathbf{v}}$. If the mesh velocity $\hat{\mathbf{v}} = 0$, the *Eulerian* framework is achieved, on the other hand if $\hat{\mathbf{v}} = \mathbf{v}$, the *Lagrangian* framework is achieved. The gradient in axisymmetric formulation read as $\nabla \bullet = (\partial \bullet / \partial x, \partial \bullet / \partial r)^T$.

Boundary conditions are required to find the particular solution of the partial differential equations presented above for the solution of the two-phase flow system. Since the geometry and the flow variables are assumed to be independent of the rotation angle θ, a symmetry boundary condition of

$$v = 0 \qquad \text{and} \qquad \frac{\partial u}{\partial r} = 0 \tag{5}$$

is required on the symmetry axis $(r = 0)$. Since the flow of the present study is driven by gravitational effects, the *no-slip* condition is used at all the remaining walls except the exit wall where pressure is set to a reference value.

3. FINITE ELEMENT METHOD

3.1 Weak Form of the Navier-Stokes Equations

If the Galerkin method is applied to the Navier-Stokes equations, one has to find $(u, v, p) \in \mathcal{U}_{u_D} \times \mathcal{V}_{v_D} \times \mathcal{Q}$ such that

$$M\left(\rho \frac{D\mathbf{v}v}{Dt}, \mathbf{v}w\right) + \frac{1}{N^{1/2}} K\left(\mathbf{v}v, \mathbf{v}w\right) + G\left(p, \mathbf{v}w\right) = M\left(\rho\, \mathbf{v}g, \mathbf{v}w\right) + \frac{1}{Eo} G(H, \kappa \mathbf{v}w)$$
$$D\left(q, \mathbf{v}v\right) = 0.$$

for all $(\mathbf{v}w, q) \in \mathcal{U}_0 \times \mathcal{V}_0 \times \mathcal{Q}$. The following bilinear forms are introduced:

$$\begin{aligned}
M\left(\mathbf{v}v, \mathbf{v}w\right) &= \int_\Omega \mathbf{v}w \cdot \mathbf{v}v \; d\mathbf{v}x, \\
K\left(\mathbf{v}v, \mathbf{v}w\right) &= 2 \int_\Omega \mu\, \mathcal{D}(\mathbf{v}w) : \mathcal{D}(\mathbf{v}v)\, d\mathbf{v}x, \\
G\left(q, \mathbf{v}w\right) &= \int_\Omega \mathbf{grad}\, q \cdot \mathbf{v}w \; d\mathbf{v}x, \\
D\left(q, \mathbf{v}w\right) &= G\left(q, \mathbf{v}w\right),
\end{aligned} \tag{6}$$

where $2\,\mathcal{D}(\mathbf{v}v) = \mathbf{grad}\, \mathbf{v}v + \mathbf{grad}\, \mathbf{v}v^T$. A procedure similar to the one described in the previous section has been used to obtain the weak form. Integrating the viscous stress tensor $\overline{\overline{\tau}}_v = 2\,\mu\,\mathcal{D}(\mathbf{v}v)$ by parts allows for transfer of the derivatives to the test function $\mathbf{v}w$. No boundary term appears because we consider only homogeneous Neumann boundary conditions for the viscous stress tensor. Therefore, the boundary $\partial\Omega$ of Ω is composed of two distinct regions $\partial\Omega_D$, $\partial\Omega_N$ on which Dirichlet and Neumann boundary conditions hold respectively:

$$\begin{aligned}
\mathbf{v}v &= \mathbf{v}v_D \quad \text{on} \quad \partial\Omega_D, \\
\overline{\overline{\tau}}_v \mathbf{v}n &= 0 \quad \text{on} \quad \partial\Omega_N.
\end{aligned}$$

The function spaces $\mathcal{U}_{u_D}, \mathcal{V}_{v_D}$ and $\mathcal{Q}$ are defined as

$$\begin{aligned}
\mathcal{U}_{u_D} &:= \{\, u \in H^1(\Omega) \mid u = u_D \quad \text{on} \quad \partial\Omega_D\}, \\
\mathcal{V}_{v_D} &:= \{\, v \in H^1(\Omega) \mid v = v_D \quad \text{on} \quad \partial\Omega_D\}, \\
\mathcal{Q} &:= \{\, q \in L^2(\Omega) \mid \int_\Omega q\, d\mathbf{v}x = 0\}.
\end{aligned}$$

Tacking the pressure function space with zero average makes the solution unique. Otherwise the pressure p could not be determined uniquely, since only derivatives of the pressure appear in the equations and the addition of a constant to the pressure would still give a solution. What is usually done numerically instead of requiring the pressure to have zero average is to fix the pressure value at an arbitrary point of the domain.

The axisymmetric case differs slightly from the Cartesian one and requires the introduction of so called weighted function spaces Belhachmi (2006); Deparis (2004). Consider the space $L^2_\alpha(\Omega)$ for any $\alpha \in \mathbb{Z}$ to be composed of functions w for which

$$\int_\Omega w^2\, r^\alpha \, d\mathbf{v}x \;\; < \;\; \infty,$$

where $d\mathbf{v}x = dx\, dr$. The subspace $\mathcal{Q}$ of $L^2_1(\Omega)$ is defined as

$$\mathcal{Q} \;\; := \;\; \{\, q \in L^2_1(\Omega) \mid \;\; \int_\Omega q\, r\, d\mathbf{v}x \;\; = \;\; 0\}.$$

Furthermore, consider the space $H^1_1(\Omega)$ as being the space of functions in $L^2_1(\Omega)$ such that their first partial derivatives are also in $L^2_1(\Omega)$. The spaces $\mathcal{U}_{u_D}, \mathcal{V}_{v_D}$ are defined as

$$\begin{aligned}
\mathcal{U}_{u_D} &:= \{\, u \in H^1_1(\Omega) \mid u = u_D \quad \text{on} \quad \Gamma_D\}, \\
\mathcal{V}_{v_D} &:= \{\, v \in H^1_1(\Omega) \mid v \in L^2_{-1}(\Omega) \quad \text{and} \quad v = v_D \quad \text{on} \quad \Gamma_D\}.
\end{aligned}$$

The bilinear forms of the axisymmetric Navier-Stokes are given by:

$$\begin{aligned}
M\,(\mathbf{v}v, \mathbf{v}w) &= \int_\Omega \mathbf{v}w \cdot \mathbf{v}v \; r\, d\mathbf{v}x, \\
K\,(\mathbf{v}v, \mathbf{v}w) &= 2\int_\Omega \mu\, \mathcal{D}(\mathbf{v}w) : \mathcal{D}(\mathbf{v}v)\, r\, d\mathbf{v}x + 2\int_\Omega \mu \frac{w_2 v}{r}\, d\mathbf{v}x, \\
G\,(q, \mathbf{v}w) &= \int_\Omega \mathbf{grad}\, q \cdot \mathbf{v}w \; r\, d\mathbf{v}x, \\
D\,(q, \mathbf{v}v) &= \int_\Omega q\, \mathbf{v}\nabla \cdot \mathbf{v}v\, r\, d\mathbf{v}x + \int_\Omega q\, v\, d\mathbf{v}x.
\end{aligned} \tag{7}$$

3.2 Elements for the Navier-Stokes Equations

When the Navier-Stokes equations are solved using the FEM, the spatial domain Ω is subdivided into finite elements and the solution is sought in finite dimensional subspaces of $\mathcal{U}_{u_D}, \mathcal{V}_{v_D}$ and $\mathcal{Q}$. These discrete subspaces are denoted $\mathcal{U}^h_{u_D}, \mathcal{V}^h_{v_D}, \mathcal{Q}^h$ and they are composed of continuous functions which are piecewise-polynomials.

A combination of velocity/pressure shape functions is usually denoted as $PnPm$, where n stands for the degree of the velocity interpolation and m stands for the degree of the pressure interpolation. For the Navier-Stokes equations, not all velocity/pressure shape function pairs lead to a stable discretization method. The shape function pairs must satisfy a compatibility condition, which is called the LBB (The LBB condition is named after Ladyzhenskaya, Babuska and Brezzi who determined it) condition or inf-sup condition Donea (2003). The solution of the Navier-Stokes equations with shape function pairs that do not fulfil the LBB condition is also possible. In this case however, additional stabilization terms have to be added to the equations. This approach called stabilized FEM, is not considered further in this text.

Several combinations of velocity/pressure shape functions have been demonstrated to fulfill the LBB condition. Some stable shape function pairs are listed in Tab (1). The $P1^{bubble}P1$ pair was introduced by Brezzi (1984) and interpolates the pressure by linear shape functions and the velocity by linear shape functions enriched by a cubic bubble function, with the control point at the element centroid. It is also called the mini element because it is the pair that fulfills the LBB condition with the lowest number of degrees of freedom per element.

Table 1. Shape function pairs satisfying the LBB condition.

name	velocity shape functions	pressure shape functions
$P1^{bubble}P1$:	linear + cubic bubble	linear
$P2P1$:	quadratic	linear
$P2^{bubble}P1$:	quadratic + cubic bubble	linear
$P3P1$:	cubic	linear

Figure. 1 displays an overview of the elements used in this work. As can be seen, many different combinations can be used in two-phase flow problems using axissymetric coordinates. The combination with the linear element enriched with

a bubble function produces stable results with low computational demand. On the other hand, the cubic element computes more accurate results with an extra computational effort.

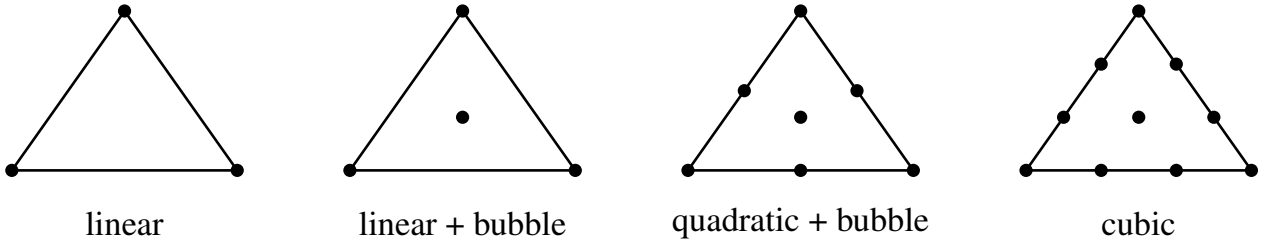

Figure 1. Interpolation nodes for triangular finite elements used in this work.

3.2.1 Linear Element

Linear finite elements are the most commonly used. For a linear triangular element, the variable is interpolated at the triangle vertex. The linear shape functions are equal to the three barycentric coordinates:

$$N_i = \lambda_i$$

3.2.2 Linear + Cubic Bubble

The linear element with cubic bubble function uses three shape functions that are interpolatory at the vertex of the element supplemented by a cubic bubble function, which is interpolatory at the element centroid. Since only four degrees of freedom are used for a cubic polynomial, the shape functions of this element are incomplete. That is, they do not span the space of third order polynomials. However, cubic bubble functions are useful for mixed interpolations where they are used for the velocity in combination with linear shape functions for the pressure. Such a scheme gives an LBB stable element without having to introduce too many degrees of freedom. The shape functions, in terms of barycentric coordinates, are:

$$\begin{aligned} N_i &= \lambda_i - 9\lambda_1\lambda_2\lambda_3 \qquad i = 1,2,3 \\ N_4 &= 27\lambda_1\lambda_2\lambda_3 \end{aligned}$$

3.2.3 Quadratic + Cubic Bubble

For the quadratic element with cubic bubble function seven interpolation points are used where six points are located at the the vertex points and the middle coordinate of each triangle, however this element is enriched by the bubble function with an extra point located at the element centroid. The shape functions, in terms of barycentric coordinates, are:

$$\begin{aligned} N_i &= \lambda_i(2\lambda_i - 1) + 3\lambda_1\lambda_2\lambda_3 \qquad i = 1,2,3 \\ N_4 &= 4\lambda_1\lambda_2 - 12\lambda_1\lambda_2\lambda_3 \qquad N_5 = 4\lambda_2\lambda_3 - 12\lambda_1\lambda_2\lambda_3 \qquad N_6 = 4\lambda_1\lambda_3 - 12\lambda_1\lambda_2\lambda_3 \\ N_7 &= 27\lambda_1\lambda_2\lambda_3 \end{aligned}$$

3.2.4 Cubic Element

For the cubic element ten interpolation points are needed where three points are located at the vertices of the element, six others are located at the edge and the last point are placed in the element centroid. This element spans the space of third order polynomials, and it is indeend the most expensive in terms of computational resources since the total number of mesh nodes is higher if compared to the previous elements. The shape functions, in terms of barycentric coordinates, are:

$$\begin{aligned} N_i &= \frac{1}{2}(3\lambda_i - 1)(3\lambda_i - 2)\lambda_i \qquad i = 1,2,3 \\ N_4 &= \frac{9}{2}\lambda_1\lambda_2(3\lambda_1 - 1) \qquad N_5 = \frac{9}{2}\lambda_1\lambda_2(3\lambda_2 - 1) \qquad N_6 = \frac{9}{2}\lambda_2\lambda_3(3\lambda_2 - 1) \\ N_7 &= \frac{9}{2}\lambda_2\lambda_3(3\lambda_3 - 1) \qquad N_8 = \frac{9}{2}\lambda_1\lambda_3(3\lambda_3 - 1) \qquad N_9 = \frac{9}{2}\lambda_1\lambda_3(3\lambda_1 - 1) \\ N_{10} &= 27\lambda_1\lambda_2\lambda_3 \end{aligned}$$

4. RESULTS

This section describes numerical results for incompressible two-phase flows obtained with the present Arbitrary Lagrangian-Eulerian Finite Element code in axisymmetric coordinate. A number of single phase flow benchmark tests were carried out to successfully validate the code, these included a *Poiseuille* flow and *Drop under uniform translation* as can be seen in Gros *et al.*.

5. Oscillating drop

The evolution of a single drop initially perturbed in its shape is presented below. This case is part of the set of standard benchmarks tests required to evaluate the modeling of the surface tension force. The simulation consists of an initially axisymmetric ellipsoidal drop immersed in another fluid in the absence of gravity. Due to the absence of external forces and assuming the viscous effects to be small, the oscillating process is mainly driven by interfacial forces which are directly balanced by the convection term. The perturbed drop tends to oscillate with the frequency given by:

$$w^2 = \frac{24\sigma}{(3\rho_{in} + 2\rho_{out})R^3} \tag{8}$$

and an amplitude decay given by:

$$a(t) = a_0 e^{-t/\tau} \tag{9}$$

where ρ_{in} stands for the drop density, ρ_{out} represents the density of the surrounding fluid and R is the unperturbed drop radius. In the amplitude equation, a_0 is the initial drop amplitude that should be small enough to avoid the growth of undesired non-linear modes. The time is given by t and $\tau = R/5\nu$ where R is the unperturbed drop radius and ν is the kinematic viscosity. For this simulation a_0 was set to $0.1R$, assuring the requirements of the linearization process.

The non-dimensional parameters used for this simulation were $\sigma = 1$ and $R = 0.5$ as the drop's radius, $\rho_{in} = 1.0$, $\mu_{in} = 1.0$ for the drop and $\rho_{out} = 0.001$ and $\mu_{out} = 0.001$ for the external fluid. The domain limits were set to be $8D$x$8D$x$8D$. The coarse mesh had approximately 8000 triangles and 12200 nodes. The interface mesh had approximately 680 line segments and 679 nodes.

Figure (2) shows the numerical solution of the interface's axial position for two different mesh refinement levels, namely coarse and refined. A comparison is then made with the analytical curve given by:

$$y(t) = y_0 + a_0 e^{-t/\tau} cos(wt). \tag{10}$$

In the above equation, y_0 corresponds to the initial oscillating surface's axial position. As expected, the predicted curve for the refined mesh has a better agreement to the analytical solution when compared to the coarse mesh. Moreover, the numerical oscillating frequency found for the refined mesh shows very good agreement to the analytical solution with an error $< 1\%$ while the coarse mesh presents an error of 4%.

5.1 Rayleigh-Taylor Instability

A case with strong interface deformation is going to be investigated. It is described by the unstable situation of a heavy fluid resting upon a lighter one in a gravitational field. The density ratio of the fluids is 0.1383 and their viscosities are equal. This case is two-dimensional and no surface tension acts on the interface. A rectangular domain of dimensions 1×4 was used. The interface is initialized with a sinusoidal perturbation of amplitude 0.05. Symmetry boundary conditions were used on all domain boundaries. The non-dimensional numbers are $Re = 391.37$ and $Fr = 0.31928$.

The same conditions were simulated by Lopez *et al.* (2005) using an interface capturing method and by Popinet and Zaleski (1999) using a front tracking algorithm. The present results for the shape of the interface are displayed in fig. (3).

The instability develops a typical mushroom shape. At larger times, thin filaments are generated which are clearly resolved by the mesh. Qualitative agreement is found when comparing fig. (3) with the figures 9 and 10 in Popinet and Zaleski (1999). In fig. (3) the present shapes are compared to those found in fig. (14) from reference Lopez *et al.* (2005). The observed agreement demonstrates that the present method works also for cases with strong interface deformation.

5.2 Rising Bubble

The numerical results were compared to the widely cited experiments performed by Bhaga and Weber (1981) and to the 3-dimensional code (Anjos (2012)) based on the same methodology here presented. Tests were carried out to predict the terminal velocity of a rising air bubble in aqueous sugar solutions for five different viscosities. According to the

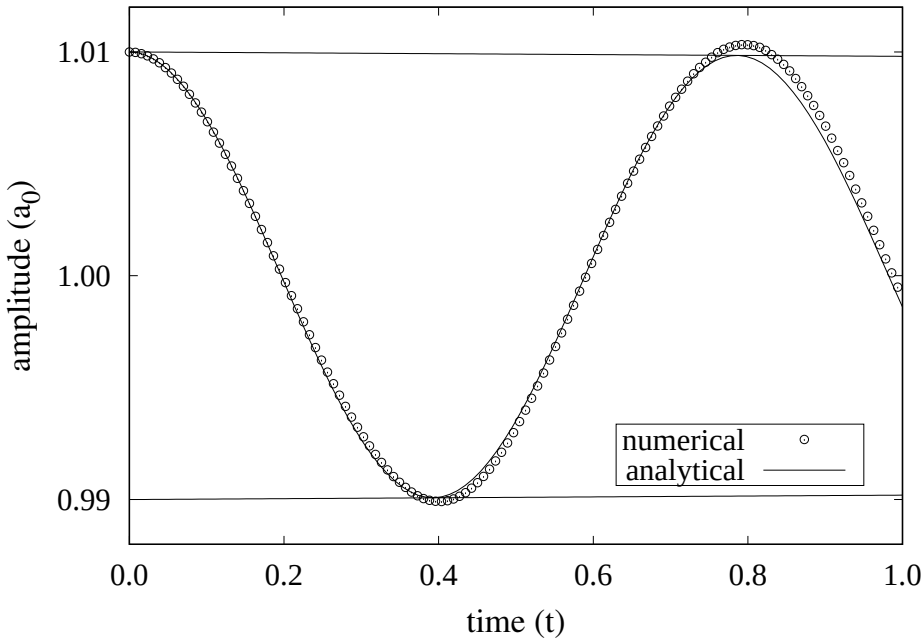

Figure 2. Comparison between numerical and analytical solution for two levels of mesh refinement. The analytical period is 0.785 and the decay rate is shown by the envelope represented by the lines below and above the oscillating curve. The oscillating period in the coarse mesh was found to be 0.820 for the coarse mesh while that for the refined mesh was 0.783.

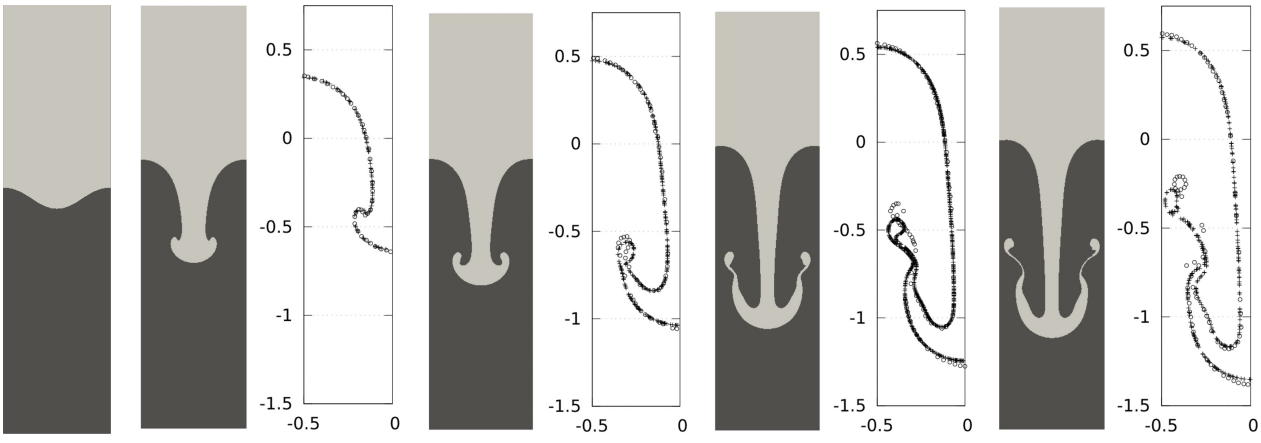

(a) $t = 0.0$ (b) $t = 0.2$ (c) $t = 0.6$ (d) $t = 0.8$ (e) $t = 0.9$

Figure 3. Interface shape at different instants in the Rayleigh-Taylor instability test and its comparison with data.

experiments, the volume of the generated bubbles was $9.3cm^3$, thus the diameter is $d = 2.61cm$. The surface tension of $0.078N/m$ was that of the air-water-sugar interface, the bubble air's viscosity and density are $0.0000178kg/ms$ and $1.225kg/m^3$ respectively. We considered an average value for the aqueous solution density to be $1350kg/m^3$, since the experiments presented measurement variations, and five different liquid viscosities $\{2.73, 1.28, 0.54\}kg/ms$, thus changing the final shape of the rising bubbles. The refinement levels used had approximately 2000 nodes, 3100 triangles, 350 interface nodes and 351 interface lines. The geometry of the domain consisted in a retangle with dimensions of $8Dx6D$ with the higher dimension along the gravity direction was used and a bubble with radius $R = 0.5$ was placed in the bottom of the domain where the center of mass is located at $y = 2$.

Figure (4) shows bubble shape transition and the center of mass velocity of the rising air bubble immersed in sugar water solution. The bottom edge of the bubble, where the curvature changes its sign varies acordingly to the viscosity.

Table 2. Fluid properties for the rising of air Taylor bubble

fluid	properties			dimensionless number		film thickness
	ρ $[kg/m^3]$	μ $[\mu Pa \cdot s]$	σ $[mN/m]$	Eo [-]	Mo [-]	δ [-]
sucrose	1.172	5.650	77.7	40	1E-07	0.0617
glycerol	1.260	712.0	63.1	40	1E-01	0.1483
diluted glycerol	0.234	154.0	64.8	100	1E-02	0.1196
air	1.789	1.225	—	—	—	—

The mesh parameters used in these simulations were $\beta_1 = 0.0$, $\beta_2 = 0.8$, $\beta_3 = 0.1$ for the volumetric mesh and $\gamma_1 = 1.0$ and $\gamma_2 = 0.1$ for the surface mesh. The Eötvs̈ number was constant for all simulations and were set to $Eo = 116$. For each case, the Archimedes number changes due to the viscosity of the liquid, as the ratio of density and viscosity as follows: case 1 $N = 194.88$, $\rho_{in}/\rho_{out} = 0.0009$, $\mu_{in}/\mu_{out} = 6.53E-06$. Case 2 $N = 194.88$, $\rho_{in}/\rho_{out} = 0.0009$, $\mu_{in}/\mu_{out} = 1.39E-05$. Case 3 $N = 1091.57$, $\rho_{in}/\rho_{out} = 0.0009$, $\mu_{in}/\mu_{out} = 3.29E-05$.

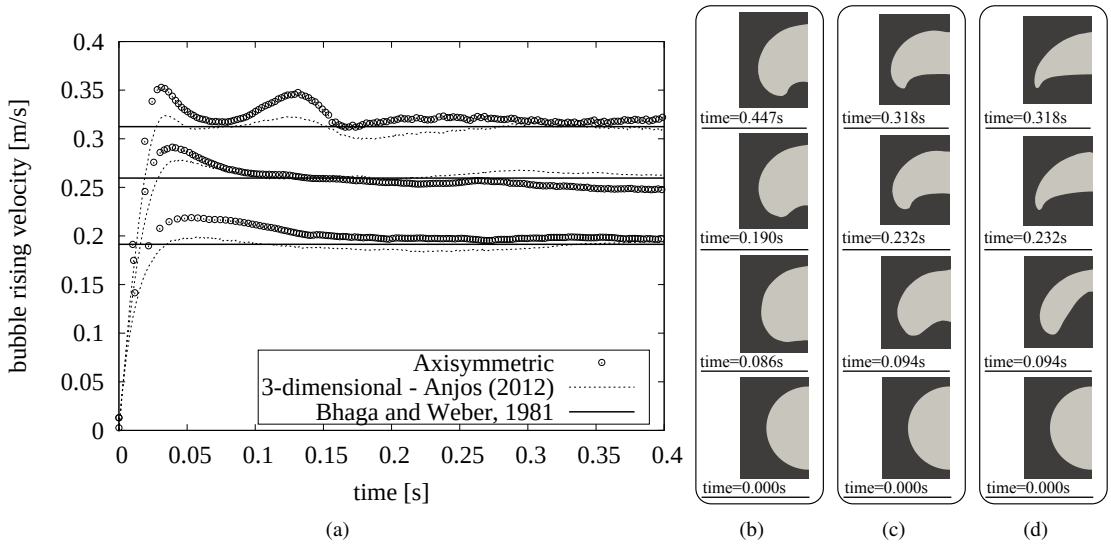

Figure 4. Time evolution of rising of an air bubble immersed in aqueous sugar solution. (a) Bubble rising velocity for three test cases and comparison with experiments performed by Bhaga and Weber (1981) and a 3D code by Anjos *et al.* (2014a). (b) $\mu = 2.73$kg/ms, (c) $\mu = 1.27$kg/ms and (d) $\mu = 0.539$kg/ms

5.3 Rising of Taylor air bubble

To characterize the rising velocity of air bubbles in different solutions, we identified 3 regions in the flow pattern map for the numerical simulations. Two solutions of glycerol and one of sucrose has been used. Table 2 summarizes the fluid properties used in the rising Taylor (elongated) bubble simulations. The $(P_2^{bubble}; P_1)$ (quad + bubble element) has been used at all simulations of the rising of Taylor air bubble.

The numerical solution for the rising bubble requires a long domain to be compatible to the experiments. According to Bugg *et al.* (1998), the development of the bubble's shape and, consequently, the terminal velocity requires that the numerical domain should be $8D$ long in the gravity direction. As mentioned before, an extra mesh refinement is needed to solve the liquid film formed between the wall and the confined bubble, thus the total number of mesh elements increases dramatically. Considering that the simulations are performed in 3-dimensions and the experimental test section is constant in the gravity direction, a moving referential frame technique is employed to shorten the numerical domain, thus allowing a faster computation.

The numerical domain used to simulate all the fluids given by Table (2) was set to $D \times 5D + L_b$, where D stands for the circular channel diameter and L_b is the bubble length. The bubble was placed far from the bottom part of the domain to guarantee that the bubble's wake is well captured, thus allowing the bottom of the bubble to deform.

Figure (5) shows the time progression of a Taylor air bubble immersed in a sucrose solution. The same bubble shape and film thickness, as the previous cases, is used as an initial shape. In the transient evolution, the bubble's velocity reached its maximum velocity at time $t \approx 1$, and its terminal velocity at time $t \approx 3.7$ Also, it was shown that the bottom part of the bubble was pulled in and oscillated until convergence at $t \approx 7.4$ The mesh parameters used in this simulation were $\beta_1 = 0.0$, $\beta_2 = 1.0$, $\gamma_1 = 1.0$ and $\gamma_2 = 0.1$ and the dimensionless numbers were set to $Mo = 1e-7$, $Eo = 40$. Figure (6 presents the transient solution of the bubble's center of mass velocity. It was observed, an overshooting of the ascension velocity from time $t = 0$ to $t = 1.1$, due to the initial deformation of the bottom part of the bubble, and consequently acceleration of the center of mass. The result agreed to the prediction of the flow pattern map, obtaining an error of 1.1%.

(a) $t = 0.13$ (b) $t = 1.99$ (c) $t = 3.24$ (d) $t = 4.09$ (e) $t = 12.00$

Figure 5. Bubble shape evolution with time for an air bubble in a sucrose solution with dimensionless numbers $Mo = 1e-7$, $Eo = 40$. (a) Initial bubble shape with $t = 0.13$. (b-d) Bubble shape change during transient solution. (e) Terminal bubble shape with $t = 12.00$.

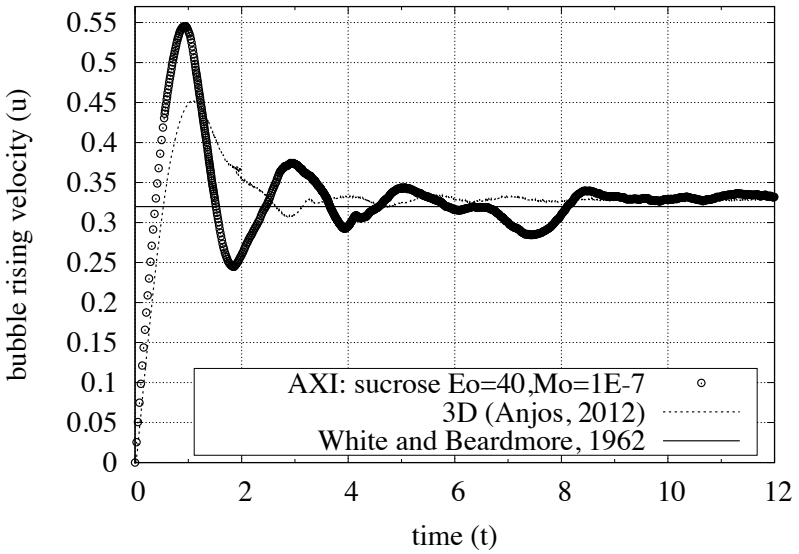

Figure 6. Rising of an air Taylor bubble immersed in a sucrose solution with dimensionless numbers set to $Mo = 1e-7$ and $Eo = 40$. The time evolution of the Bubble's center of mass velocity is compared to the terminal bubble's velocity found in White and Beardmore (1962). Velocity and time are non-dimensional.

Figure (7) show the evolution in time of the bubble's center of mass velocity, in which the computed terminal velocity approaches the value found in the flow pattern map. The error was found to be 6.5%. The mesh parameters used in this simulation were $\beta_1 = 0.0$, $\beta_2 = 0.5$, $\gamma_1 = 0.5$ and $\gamma_2 = 0.1$ and the pair of dimensionless numbers was set to

$Mo = 1e-2$,$Eo = 100$ and $Mo = 1e-1$,$Eo = 40$. In this case, the mesh parameters were slightly modified to test different mesh conditions in the simulation. The obtained result shows that the bubble shape and terminal velocity agrees well to experimental data.

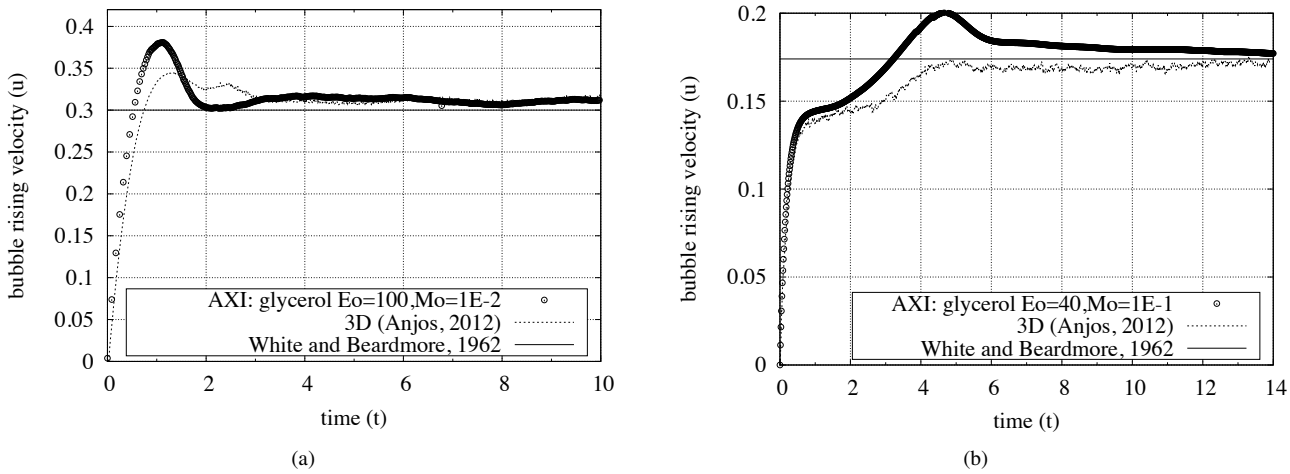

Figure 7. Rising of an air Taylor bubble immersed in a glycerol solution with dimensionless pair numbers set to (a) $Mo = 1e-2$,$Eo = 100$ and (b) $Mo = 1e-1$,$Eo = 40$. The time evolution of the Bubble's center of mass velocity is compared to the terminal bubble's velocity found in White and Beardmore (1962). Velocity and time are non-dimensional.

At our simulations, the film thickness of the rising of the Taylor bubbles presented errors of $4-6\%$ compared to the correlation of Brown (1965). It is important to note that the liquid film for the Taylor bubble simulations adds significantly the difficult of handling the mesh in the liquid film. However, with the proposed adaptive mesh refinement, the dynamics of the bubble rise could be essentially captured.

6. CONCLUSIONS

In this article, a moving mesh interface tracking method was presented for the simulation of axisymmetric two-phase flows. This method discretizes the incompressible Navier-Stokes equations with the finite element method on unstructured triangular meshes. The equations and partial results were described in details. An adaptive mesh refinement method was used to accurately resolve the interface motion and remeshing was performed to preserve the quality of the mesh elements. The point distribution was obtained by solving a Helmholtz equation based on a desired edge length density field. Mesh points are automatically inserted/removed based on the ratio of edge length to desired edge length. Using a discrete version of the Frenet-Serret formula for the curvature calculation was proved to be a good choice, as high accuracy could be achieved at very low computational cost. Validation of the method was presented for two-phase flow problems including the rising of single bubbles where the numerical results were compared to experimental data. Based on the presented results, the current approach was shown to be an accurate simulations tool for capillary two-phase flows.

7. ACKNOWLEDGEMENTS

The authors would like to thank the European Union funded THERMAPOWER (Thermal Management of High Power Microsystems using Multiphase Flows) project (reference 294905) for partially supporting this work. G. R. Anjos also thanks the FAPERJ (Research Support Foundation of the State of Rio de Janeiro) for its support.

8. REFERENCES

Anjos, G., 2012. *A 3D ALE Finite Element Method for Two-Phase Flows with Phase Change*. Ph.D. thesis, École Polytechnique Fédérale de Lausanne.

Anjos, G., Borhani, N., Mangiavacchi, N. and Thome, J., 2014a. "3d moving mesh finite element method for two-phase flows". *Journal of Computational Physics*, Vol. 270, pp. 366–377. doi:10.1016/j.jcp.2014.03.067.

Anjos, G., Mangiavacchi, N. and Pontes, J., 2014b. "Three-dimensional finite element method for rotating disk flows". *Journal of the Brazilian Society of Mechanical Sciences and Engineering*, Vol. 36, No. 4, pp. 709–724. doi: 10.1007/s40430-013-0120-0.

Bhaga, D. and Weber, M., 1981. "Bubbles in viscous liquids: Shapes, wakes and velocities". *Journal of Fluid Mechanics*, Vol. 105, pp. 61–85.

Brackbill, J. and Kothe, D., 1992. "A continuum method for modeling surface tension". *Journal of Computational Physics*, Vol. 100, pp. 335–354.

Brown, R., 1965. "The mechanism of large bubbles intubes. i. bubbles velocities in stagnant liquids". *Canadian Journal of Chemical Engineering*, Vol. 43, pp. 217–223.

Bugg, J., Mack, K. and Rezkallah, K.S., 1998. "A numerical model of taylor bubbles rising through stagnant liquids in vertical tubes". *International Journal of Multiphase Flow*, Vol. 24, pp. 271–281.

Gros, E., Anjos, G.R. and Thome, J.R., ???? "Interface-fitted moving mesh method for axisymmetric two-phase flow in microchannels". *International Journal for Numerical Methods in Fluids*, pp. 1–17. ISSN 1097-0363. doi: 10.1002/fld.4413. URL `http://dx.doi.org/10.1002/fld.4413`. Fld.4413.

Lopez, J., Hernandez, J., Gomez, P. and Faura, F., 2005. "An improved plic-vof method for tracking thin fluid structures in incompressible two-phase flows". *Journal of Computational Physics*, Vol. 208, pp. 51–74. doi: 10.1016/j.jcp.2014.03.067.

Popinet, S. and Zaleski, S., 1999. "Front tracking algorithm for accurate representation of surface tension". *International Journal for Numerical Methods in Fluids*, Vol. 30, pp. 775–793.

White, E. and Beardmore, R., 1962. "The velocity of rise of single cylindrical air bubbles through liquids contained in vertical tubes". *Chemical Engineering Science*, Vol. 17, pp. 351–361.

Anjos, G.R. (2012) A 3D ALE Finite Element Method for Two-Phase Flows with Phase Change, Ph.D. thesis, EPFL.

Anjos, G.R.; Borhani, N.; Mangiavacchi, N.; Thome J.R. (2014) A 3D moving mesh Finite Element Method for two-phase flows, *Journal of Computational Physics*, **270**: 366-377.

Batchelor, G.K. (2000) An Introduction to Fluid Dynamics, *Cambridge University Press.*

Balcazar, N.; Lehmkuhl, O.; Jofre, L.; Rigola, J.; Oliva, A. (2016) A coupled volume-of-fluid/level-set method for simulation of two-phase flows on unstructured meshes, *Computers and Fluids*, **124**, 12-29.

Belhachmi, Z.; Bernardi, C.; Deparis S. (2006) Weighted Clement operator and application to the finite element discretization of the axisymmetric Stokes problem, *Numerische Mathematik*, **105**, 217-247.

Brackbill, J.U.; Kothe, D.B.; Zemach C. (1992) A Continuum Method for Modeling Surface Tension, *Journal of Computational Physics*, **100**: 335-354.

Arnold, D.N.; Brezzi, F.; Fortin M. (1984) A stable finite element for the Stokes equations, *Calcolo*, **21**, 337-344.

Chiandussi, G.; Bugeda, G.; Onate, E. (2000) A simple method for automatic update of finite element meshes, *Commun. Numer. Meth. Engng.*, **16**, 1-19.

Deparis S. (2004) Numerical Analysis of Axisymmetric Flows and Methods for Fluid-Structure Interaction Arising in Blood Flow Simulation, Ph.D. thesis, EPFL.

Donea, J.; Huerta, A. (2003) Finite element methods for flow problems, *John Wiley & Sons*, Ltd.

Donea, J.; Huerta, A.; Rodriguez-Ferran, A.; Ponthot, J.-Ph. (2004) Arbitrary Lagrangian-Eulerian Methods, *Encyclopedia of Computational Mechanics Vol 1 Chap. 14*, John Wiley & Sons.

Ganesan, S.; Tobiska, L. (2008) An accurate finite element scheme with moving meshes for computing 3D-axisymmetric interface flows, *Int. J. Numer. Meth. Fluids*, **57**, 119-138.

Ganesan, S. (2006) Finite element methods on moving meshes for free surface and interface flows, Ph.D. thesis, Otto-von-Guericke-University Magdeburg.

Ginzburg, I.; Wittum, G. (2001) Two-Phase Flows on Interface Refined Grids Modeled with VOF, Staggered Finite Volumes, and Spline Interpolants, *J. Comput. Phys.* **166**, 302-335.

Gross, S. (2008) Numerical methods for three-dimensional incompressible two-phase flow problems, Ph.D. thesis, RWTH Aachen.

Gross, S.; Reusken, A. (2011) Numerical Methods for Two-phase Incompressible Flows, *Springer-Verlag Berlin Heidelberg.*

Hirt, C.W.; Nichols, B.D. (1981) Volume of Fluid (VOF) Method for the Dynamics of Free Boundaries, *J. Comput. Phys.*, **39**, 201-225.

Johnson, A.A.; Tezduyar, T.E. (1994) Mesh update strategies in parallel finite element computations of flow problems with moving boundaries and interfaces, *Comput. Methods Appl. Mech. Engrg.*, **119**, 73-94.

Juric, D.; Tryggvason, G. (1998) Computations of Boiling Flows, *Int. Journal of Multiphase Flow*, **24**, 387-410.

Khodaparast, S.; Magnini, M.; Borhani, N.; Thome, J.R. (2015) Dynamics of isolated confined air bubbles in liquid flows through circular microchannels: an experimental and numerical study, *Microfluidics and Nanofluidics*, **19**, 209-234.

Lamb, H. (1916) Hydrodynamics, Fourth Edition, *Cambridge University Press.*

Lopez, J.; Hernandez, J.; Gomez, P.; Faura, F. (2005) An improved PLIC-VOF method for tracking thin fluid structures in incompressible two-phase flows, *J. Comput. Phys.*, **208**, 51-74.

Magnini, M.; Pulvirenti, B; Thome, J.R. (2016) Characterization of the Velocity Fields Generated by Flow Initialization in the CFD Simulations of Multiphase Flows, *Applied Mathematical Modelling*, **40**, 6811-6830.

Masud, A.; Hughes, T.J.R. (1997) A space-time Galerkin/least-squares finite element formulation of the Navier-Stokes equations for moving domain problems, *Comput. Methods Appl. Mech. Engrg.*, **146**, 91-126.

Murea, C.M. (2010) Arbitrary Lagrangian Eulerian approximation with remeshing for Navier-Stokes equations, *Int. J. Numer. Meth. Biomed. Engng.*, **26**, 1435-1448.

Pironneau, O. (1982) On the Transport-Diffusion Algorithm and Its Applications to the Navier-Stokes Equations, *Numerische Mathematik*, **38** ,309-332.

Popinet, S. (2009) An accurate adaptive solver for surface-tension-driven interfacial flows, *J. Comput. Phys.*, **228**, 5838-5866.

Popinet, S.; Zaleski, S. (1999) A front-tracking algorithm for accurate representation of surface tension, *Int. J. Numer. Meth. Fluids*, **30**, 775-793.

Pozrikidis, C. (2011) Introduction to Theoretical and Computational Fluid Dynamis, *Oxford University Press*, second edition.

Quan, S.; Schmidt, D.P. (2007) A moving mesh interface tracking method for 3D incompressible two-phase flow, *Journal of Computational Physics*, **221**, 761-780.

Roos, F.W.; Willmarth, W.W. (1971) Some Experimental Results on Sphere and Disk Drag, *AIAA Journal*, **9**: 285-291.

Sauerland, H. (2013) An XFEM Based Sharp Interface Approach for Two-Phase and Free-Surface Flows, Ph.D. thesis, RWTH Aachen.

Scardovelli, R.; Zaleski, S. (1999) Direct Numerical Simulation of Free-Surface and Interfacial Flow, *Annu. Rev. Fluid Mech.*, **31**, 567-603.

Schlichting, H. (1979) Boundary Layer Theory, *McGraw-Hill*, New York, 7-th edition.

Shewchuck, J.R. (1996) Triangle: engineering a 2D quality mesh generator and Delaunay triangulator, *in Applied Computational Geometry: Towards Geometric Engineering, Lecture Notes in Computer Science* **1148**, 203-222.

Stavrev, A.; Knechtges, P.; Elgeti, S.; Huerta, A. (2015) Space-time NURBS-enhanced finite elements for free-surface flows in 2D, *Int. J. Numer. Meth. Fluids* doi:10.1002/fld.4189.

Stokes, G.G. (1880-1905) On the Effect of the Internal Friction of Fluids on the Motion of Pendulums, *Transactions of the Cambridge Philosophical Society 1851, Reprinted in Mathematical and Physical Papers*, **3**.

Sussman, M.; Smereka, P.; Osher, S. (1994) A Level Set Approach for Computing Solutions to Incompressible Two-Phase Flow, *J. Comput. Phys.*, **114**, 146-159.

Tabata, M.; Itakura, K. (1998) A precise computation of drag coefficients of a sphere, *Int. J. Comput. Fluid Dynam.*, **9**: 303-311.

Tezduyar, T.E.; Behr, M.; Liou, J. (1992) A new strategy for finite element computations involving moving boundaries and interfaces - the deforming-spatial-domain/space-time procedure: I. The concept and the preliminary tests, *Comput. Methods Appl. Mech. Engrg.*, **94**, 339-351.

Tezduyar, T.E.; Behr, M.; Mittal, S.; Johnson, A.A. (1992) Computation of unsteady incompressible flows with the finite element methods - space-time formulations, iterative strategies and massively parallel implementations, *in P.S. Molinski, W.K. Liu, G. Hulbert, and K. Tamma, editors, New Methods in Transient Analysis, AMD* **143**, ASME, 7-24.

Tryggvason, G.; Bunner, B.; Esmaeeli, A.; Juric, D.; Al-Rawahi, N. (2001) A Front-Tracking Method for the Computations of Multiphase Flow, *Journal of Computational Physics*, **169**, 708-759.

Zienkiewicz, O.C.;Taylor, R.L.; Nithiarasu, P. (2014). The finite element method for fluid dynamics (Seventh Edition), *Butterworth-Heinemann.*

9. RESPONSIBILITY NOTICE

The authors are the only responsible for the printed material included in this paper.